THE NONREACTIVE ELECTRONIC QUENCHING OF NITRIC OXIDE WITH MOLECULAR OXYGEN

NAA-KWARLEY QUARTEY

The College of William & Mary

Dr. Nathanael Kidwell

Abstract: High temperature gas molecules, such as nitric oxide (NO), are prevalent in hypersonic flows. Uncertainty remains in the behavior of these molecules especially in understanding the role of NO in electronic quenching. In developing better predictions of molecule's behavior in electronic quenching, we can make a great impact improving the optimization of aerospace technologies. Furthermore, we present results to develop a better understanding of the behavior of NO in atmospheric photochemical processes. To these ends, we use velocity map imaging (VMI) to analyze products' total kinetic energy release (TKER) distributions and product state distributions resulting from nonreactive collision of NO with molecular oxygen (O_2). A dual flow nozzle was constructed and implemented to analyze NO collisional quenching and to limit the formation of nitrogen dioxide (NO_2). From the isotropic images that we obtained, we observed that dissociation is occurring on a much longer timescale before the formation of products. There is a deviation between the experimental and statistical prediction results, which may be due to the conical intersection's role in influencing the dynamical evolution of the system.

Introduction

Aerosols are minuscule particles that are present in marine atmospheres, Earth's atmosphere, and other planetary atmospheres. Furthermore, aerosols are present in many forms such as dust, smog, sea salt, or volcanic ash, and these organic/inorganic particulates can either come from natural or man-made substances.[1] One type of aerosol that is present in the form of nitric oxide species, called nitric oxide (NO), is valuable as a non-reactive tracer molecule in gaseous flow field characterization, either naturally occurring in the case of high-enthalpy flows and combustion, or through seeding.[2] Furthermore, NO can easily be added to air without changing significantly the net molecular weight, and thus it is ideal as a seed species in studies involving compressible flows.[3] These molecular components have an important role in hypersonic flow. Chemical processes with high temperature gas effects can occur when vehicles are moving at hypersonic speeds or speeds moving at speeds that are five times the speed of sound. The high temperature gas effects can cause issues related to hypersonic aerodynamic design and optimization.[4] Once

the gas is at high temperature, this can lead to chemical processes where it affects the properties of the surrounding air around it which causes it to behave more as a real gas instead of an ideal one. These molecules can start dissociating at these high temperatures which causes atomic ionization to occur.[4]

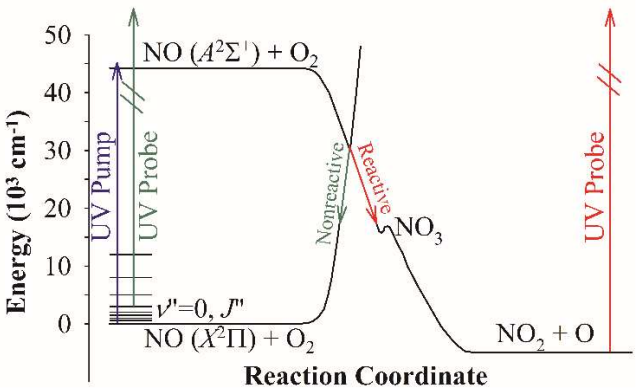

Figure 1: Reactive and Nonreactive Quenching Pathways of NO and O_2

A chemical process that NO and molecular oxygen (O_2) can encounter is called collisional quenching where NO is in its excited state and loses its energy through a collision with another molecule partner or the quencher, in this case O_2, which decreases its fluorescence.[5] Collisional quenching can take on different pathways as shown in Figure 1 known as reactive quenching, where NO and O_2 can form new products, or nonreactive quenching where NO and O_2 can be returned to their ground electronic states and respective rovibrational states. In Figure 1, for the reactive quenching pathway, a radical intermediate, nitrate (NO_3) could play a role in the quenching process before the products of nitrogen dioxide (NO_2) and oxygen atom (O) are formed. Figure 2 represents the energetically accessible levels of the quenched products that the available energy may be partitioned. Since there are still gaps present in scientific literature regarding the mechanisms of electronic quenching, we aim to understand their dynamics to better inform predictive modeling of NO in hypersonic flows.

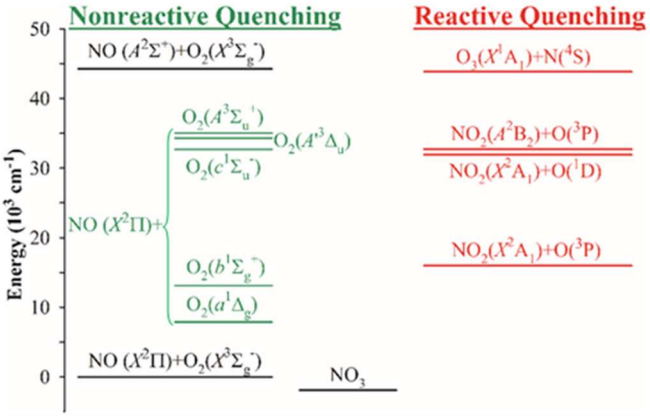

Figure 2: Energy level diagram of possible nonreactive and reactive product channels upon quenching of NO ($A^2\Sigma^+$) by O_2. For the nonreactive channel, quenching produces NO in its ground $X^2\Pi$ electronic state and O_2 in its ground $X^3\Sigma_g^-$ or low-lying electronic states. Reactive quenching can lead to NO_2 + O and O_3 + N products.

Experiment

In our experiment, we use a technique called Velocity Map Imaging (VMI) that gives us valuable information to determine the velocity distribution of products arising from collisional quenching. In the setup of our experiment, which is shown in Figure 3, we pulse NO and O_2 into a high-vacuum chamber, and were designated in separate gas lines to prevent the formation of NO_2. Once the molecules enter the chamber, they undergo supersonic jet expansion to cool NO and O_2 to their lowest quantum levels. After passing the first ion optic, NO is excited to its first electronic state using a Nd:YAG pumped dye laser (Surelite II-10/NarrowScan K). Subsequently, O_2 collides with NO in its excited electronic state to initiate quenching, and we probe the formation of NO in different rovibrational states using a probe laser (Radiant Dyes, Narrow Scan). The probed NO products from collisional quenching are then

ionized with the same probe laser source, and form an ion cloud that impacts the microchannel plate (MCP) and phosphor detector. Lastly, we record an image of the NO products with the 2D detector and a charge couple device (CCD) camera to obtain the velocity distributions of NO from collisional quenching. In order to perform this experiment, we needed to modify our chamber.

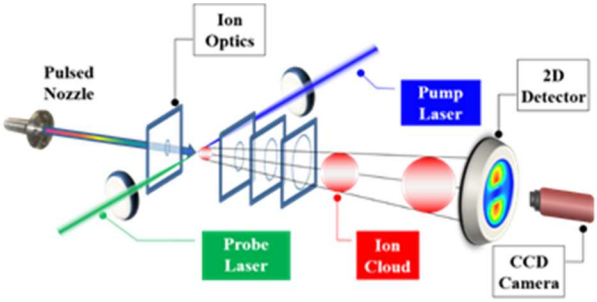

Figure 3: Velocity Map Imaging Technique used to Study Molecular Photochemistry

We assembled a dual flow nozzle[5] in our chamber shown in Figure 4 to limit NO and O_2 to intersect with each other only at the exit of the pulse valve. NO and O_2 moved separately through calibrated mass flow controllers. O_2 entered through the main sample line, and NO entered through a parallel sample line and a 'v-channel'. After both are pulsed in to the high-vacuum chamber, electronic quenching of NO is initiated.

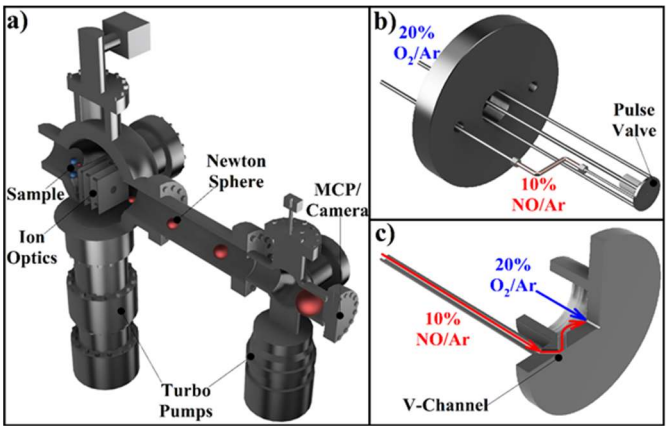

Figure 4: (a) Schematic drawing of the velocity map imaging apparatus used to study electronic quenching dynamics. (b) 10% NO/Ar and 20% O_2/Ar flow through separate gas lines to limit reaction to NO_2. (c) Close-up of the dual-flow pulse nozzle, in which NO flows through a 'v-channel' where NO encounters O_2 only at the pulse valve exit. Both reagent gases are injected into a high-vacuum chamber with supersonic jet cooling prior to the pump and probe laser pulses.

Results

Nonreactive collisional quenching is the most influential decay process for NO. Figure 5 (a) demonstrates the temporal profile that is present when the time delay is scanned between the pump and the probe laser. The pump laser excites NO to its excited state and the probe laser detects formation of NO ($X^2\Pi$, v''=0, $R_1(J''$=50.5)) while the time separation between both lasers is scanned. To determine the excited state lifetime of NO, we extrapolated a line of best fit using an exponential decay function. We observed a lifetime of $\tau = 132 \pm 1$ ns which is much shorter compared to NO's radiative lifetime of 205 ± 5 ns.[7] In Figure 5 (b), we measure an enhancement in signal of NO ($X^2\Pi$, v''=0, $R_1(J''$=50.5)) ions when the probe laser was simultaneously in use with the pump laser and

we observed no enhancement in signal when the pump laser was turned off.

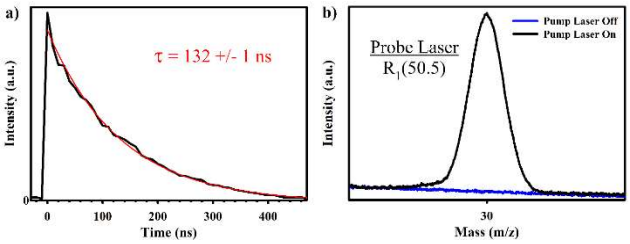

Figure 5: (a) Temporal decay profile of NO ($A^2\Sigma^+$) while monitoring the NO ($X^2\Pi$, v''=0, $R_1(J''$=50.5)) level under typical experimental conditions for electronic quenching. The pump laser populates the NO ($A^2\Sigma^+$, v'=0, J'=0.5) level and decays to NO ($X^2\Pi$) states following collisional quenching with O_2. The best-fit NO ($A^2\Sigma^+$) quenched lifetime is τ=132±1 ns while recording the probe ion signal enhancement for the NO ($X^2\Pi$, v''=0, $R_1(J''$=50.5)) level. (b) After a time delay of 50 ns, the probe laser detects NO ($X^2\Pi$, v''=0, $R_1(J''$=50.5)) products of collisional quenching. The probe ion signal enhancement is detected when the pump laser is present with the probe laser and disappears when the pump laser is off.

Energy can be partitioned in the form of translation, rotation, vibration, or electronic states. In Figure 6 on the top panel, the total kinetic energy release (TKER) in black shows the experimental results of energy partitioning to NO translation. The image to the right of the distribution shows an isotropic distribution of NO, which is indicative of collisional quenching occurring on a longer timescale than the rotational period of NO (< 1ps). The TKER on the bottom panel in red shows the distribution based on statistical Prior simulations, which is used to simulate a statistical energy partitioning following NO $A^2\Sigma^+$ electronic quenching. From the collisional quenching that occurred between NO and O_2, a significant amount of its energy is placed into O_2 rovibronic levels, while a smaller amount of available energy is placed into translation. The deviation between our experimental and statistical results is present because there is a conical intersection which is expected to significantly affect the dynamical outcomes following NO collisional quenching.

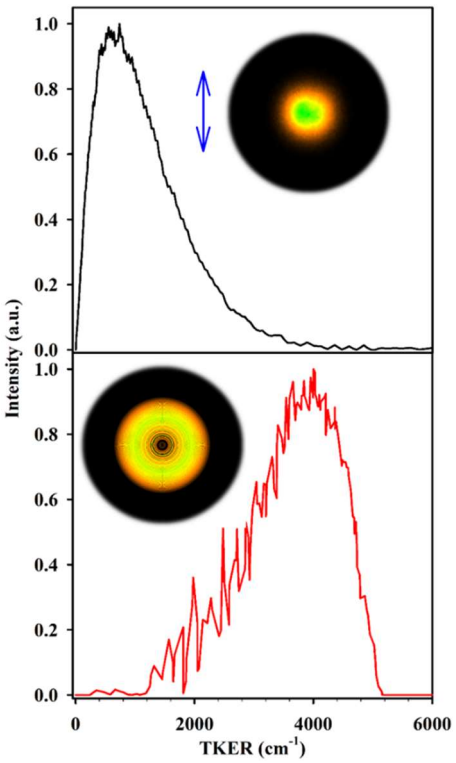

Figure 6: (Top panel) Total kinetic energy release (TKER) of NO ($X^2\Pi$, v''=0, $R_1(J''$=50.5)) and O_2 products from collisional quenching (black trace). The inset shows the ion image showing an isotropic distribution, which is consistent with electronic quenching of NO ($A^2\Sigma^+$, v'=0, J'=0) occurring on a slower timescale than the rotational period of NO. (Bottom panel) The ion image and TKER distribution (red trace) from a Prior simulation is shown for comparison and is generated assuming O_2 ($c^1\Sigma_u^-$) as the collisional co-product.

In Figure 7, we measured the rotational product state distribution of NO, and analyzed the data by also comparing the experimental results to a statistical Prior simulation. We measured the extent of rotational excitation by extracting the rotational temperature of the product state distribution using a linear Boltzmann distribution function. The rotational temperature for the Q branch (bolded) and R branch (dotted) in the various spin-orbit states, indicated as black for F_1 and red for F_2, are larger than the predicted rotational temperature calculated by the Prior simulation (3000K). This deviation is also indicative of nonstatistical behavior of NO

products, likely due to the key role of the conical intersection. Furthermore, the rotational temperature is somewhat larger for the Q-branch compared to the R-branch, which is indicative of the fact that NO π^* molecular orbital is aligned perpendicular to the molecular plane of rotation.

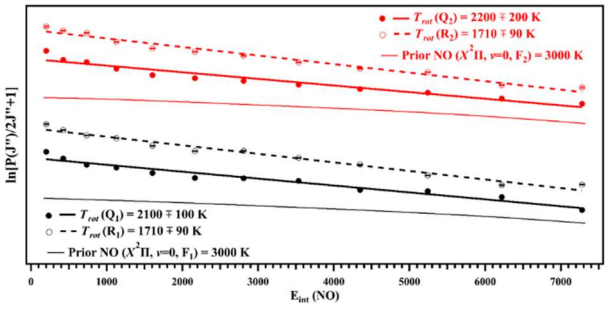

Figure 7: Product state distributions of NO ($X^2\Pi$, v''=0, J'', F_n, Λ) products from collisional quenching of NO ($A^2\Sigma^+$) with O_2. The lower F_1 (Ω=1/2) and upper F_2 (Ω=3/2) spin-orbit manifolds are represented as bold black and red traces, respectively. The Q-branches are shown as filled markers and the R-branches have open markers. The best-fit Boltzmann functions are used to extract the rotational temperature for the observed distributions. Statistical Prior simulations for the F_1 and F_2 spin-orbit levels are also shown as non-bold traces for comparison to the experimental results.

Discussion

The results from the NO ion images and product state distributions provide a deeper understanding of its quenching dynamics. From the isotropic image present, we observe that the collision of NO and O_2 causes a collisional complex to occur. This image additionally shows that the molecules rotate at a slower timescale before the NO and O_2 products are formed. From previous studies conducted, there may be a harpoon mechanism occurring where a lone pair on the NO pulls O_2 in a harpoon-like fashion to create an intermediate NO_3 complex. This NO_3 radical intermediate could undergo a roaming dissociation where intramolecular abstraction occurs by a frustrated bond cleavage which leaves part of the molecule without energy to escape and it orbits the remaining fragment until it encounters a reactive site to form the products. Its in-plane two-state roaming dynamics access multiple potential energy surfaces for NO_3 photodissociation.[6] The products from this NO_3 intermediate are NO and O_2 as shown in the nonreactive pathway in Figure 1. It is likely that the electronic quenching of NO with O_2, which proceeds through the NO_3 intermediate, evolves to products in a similar fashion as the NO_3 intermediate.

As shown in Figure 7, there is a deviation between the experimental and statistical Prior product state distributions, signifying that nonreactive quenching is therefore nonstatistical. This deviation is the outcome from the dynamical interaction between NO and O_2. According to the figure, the Q-branch levels are more populated at a larger rotational temperature compared to the R-branch levels. There is a preference for NO ($X^2\Pi$, v''=0, J'') in the $\Pi(A'')$ Λ-doublet state which corresponds to a preference for the molecular orbital to have a perpendicular orientation with respect to the molecular rotation plane.[6] Therefore, the present results are directly reporting on the conical intersection's role in populating NO ($X^2\Pi$) in a particular Λ-doublet state.

Conclusion

In understanding the role of NO and O_2 in hypersonic flow, our goals are to first have a better comprehension of the TKERs and product state distributions obtained from nonreactive and reactive collisional quenching that NO can encounter with various collisional partners. In this experiment, we specifically focused on the nonreactive product state distributions of NO and O_2 using VMI. We observed that experimentally our TKER and product state distributions were nonstatistical since they deviated from our Prior simulation calculations. There is a conical intersection

that is sampled as the products recoil from one another, which is certainly contributing to observed deviation. Along with high-level theory, future work will look into the reactive pathway of collisional quenching for NO and O_2 and characterizing the NO ($X^2\Pi$, $v''>0$) and O_2 (v', J') product state distributions and ion images in different electronic states from NO ($A^2\Sigma^+$) nonreactive quenching to quantify the branching fractions.

Acknowledgements

Acknowledgements are made to the Virginia Space Grant Consortium, K. Jacob Blackshaw, Robert T. Korb, David J. Hood, Christian D. Hettwer, and Dr. Nathanael M. Kidwell for support of this research.

References

(1) Laskin, A.; Laskin, J.; Nizkorodov, S. A. Chemistry of Atmospheric Brown Carbon. *Chem. Rev.* **2015**, *115* (10), 4335–4382. https://doi.org/10.1021/cr5006167.

(2) Mai, C. L. N.; West, N. A.; Eveland, W. D.; Bowersox, R. D. W.; Sánchez-González, R.; North, S. W. Low-Temperature Collisional Quenching of NO A 2 Σ + (v′ = 0) by NO(X 2 Π) and O 2 between 34 and 109 K . *J. Chem. Phys.* **2014**, *141* (7), 074313. https://doi.org/10.1063/1.4892980.

(3) Zhang, R.; Crosley, D. R. Temperature Dependent Quenching of A 2Σ+ NO between 215 and 300 K. *J. Chem. Phys.* **1995**, *102* (19), 7418–7424. https://doi.org/10.1063/1.469054.

(4) Emelyanov, V.; Karpenko, A.; Volkov, K. Simulation of Hypersonic Flows with Equilibrium Chemical Reactions on Graphics Processor Units. *Acta Astronaut.* **2019**, No. December 2018, 1–13. https://doi.org/10.1016/j.actaastro.2019.01.010.

(5) Nava, M.; Martin-Drumel, M. A.; Lopez, C. A.; Crabtree, K. N.; Womack, C. C.; Nguyen, T. L.; Thorwirth, S.; Cummins, C. C.; Stanton, J. F.; McCarthy, M. C. Spontaneous and Selective Formation of HSNO, a Crucial Intermediate Linking H2S and Nitroso Chemistries. *J. Am. Chem. Soc.* **2016**, *138* (36), 11441–11444. https://doi.org/10.1021/jacs.6b05886.

(6) Greenstock, C. L.; Helman, W. P.; Ross, A. B.; Tsang, W.; Bragg, A. E.; Kammrath, A.; Cheshnovsky, O.; Neumark, D. M.; Rossky, P. J.; Turi, L.; et al. No Straight Path : Roaming in Both. **2012**, No. March, 1075–1079.

(7) Luque, J.; Crosley, D. R. Radiative and Predissociative Rates for NO $A^2\Sigma^+$ v'=0-5 and $D^2\Sigma^+$ v'=0-3 *J. Chem. Phys.* **2000**, *112*, 9411-9416.